Journal of Biomedical Optics

BiomedicalOptics.SPIEDigitalLibrary.org

Collagen density and alignment in responsive and resistant trastuzumab-treated breast cancer xenografts

Alex J. Walsh
Rebecca S. Cook
Jae H. Lee
Carlos L. Arteaga
Melissa C. Skala

SPIE.

Journal of Biomedical Optics 20(2), 026004 (February 2015)

Collagen density and alignment in responsive and resistant trastuzumab-treated breast cancer xenografts

Alex J. Walsh,[a] Rebecca S. Cook,[b] Jae H. Lee,[a] Carlos L. Arteaga,[b,c] and Melissa C. Skala[a,*]
[a]Vanderbilt University, Department of Biomedical Engineering Station B, Box 1631, Nashville, Tennessee 37235, United States
[b]Vanderbilt University, Department of Cancer Biology, Breast Cancer Research Program, 2220 Pierce Avenue, Nashville, Tennessee 37232, United States
[c]Vanderbilt University, Department of Medicine, 2220 Pierce Avenue, Nashville, Tennessee 37232, United States

Abstract. Tumor collagen characteristics influence tumor malignancy, invasion, and metastasis. This study investigates the effects of trastuzumab (Tz) on the collagen of Tz-responsive (BT474) and Tz-resistant (HR6) breast cancer xenografts. Collagen content was assessed by *in vivo* second harmonic generation (SHG) imaging and histological trichrome staining of tumor sections. Collagen SHG imaging of control BT474 and HR6 tumors demonstrated increased collagen density after 14 days of treatment ($p < 0.05$). Trichrome staining revealed decreased collagen in Tz-treated BT474 and HR6 tumors at 2, 5, and 14 days of treatment, suggesting that Tz affects the tumor microenvironment independent of epithelial cell response. Additionally, collagen alignment analysis revealed significantly less aligned collagen in the Tz-treated BT474 tumors at day 14 compared with control BT474 tumors. There was no correlation between SHG endpoints (collagen density and alignment) and trichrome staining ($p > 0.05$), consistent with the physically distinctive nature of these measurements. There was also no correlation between tumor size and collagen endpoints ($p > 0.05$). These results identify changes within the collagen compartment of the tumor microenvironment following Tz treatment, which are independent from the tumor cell response to Tz, and demonstrate that intravital collagen SHG imaging is capable of measuring dynamic changes in tumor microenvironment following treatment that complements trichrome staining. [DOI: 10.1117/1.JBO.20.2.026004]

Keywords: drug response; intravital imaging; multiphoton microscopy; second harmonic generation; Herceptin.

Paper 140622RR received Sep. 26, 2014; accepted for publication Jan. 21, 2015; published online Feb. 20, 2015.

1 Introduction

Collagen is an important protein within the extracellular matrix (ECM) of normal and malignant tissues. In normal breast tissue, increased collagen is associated with increased risk of developing breast cancer and increased disease aggressiveness.[1] Recent studies of intratumoral collagen demonstrate that collagen fiber alignment and density associate with aggressive disease and increased invasion.[1–3] Furthermore, a high density of interconnected collagen fibers within the ECM of tumors can block the diffusion of drugs into the tumor.[4] These studies highlight the importance of collagen within the tumor microenvironment (TME), particularly with respect to tumor invasion and drug response. They also demonstrate a need for studies that monitor dynamic changes in collagen during breast tumor progression and elucidate how intratumoral collagen may change in response to anticancer treatments.

Breast cancers are divided into three clinical subtypes: estrogen receptor (ER) positive, human epidermal growth factor receptor 2 (HER2) positive, and triple negative breast cancer (lacking expression of ER, HER2, and progesterone receptor). HER2 is overexpressed in ~20% of breast cancers, correlating with poor clinical outcome and increased tumor malignancy.[5] Fortunately, several drugs are approved for direct targeting of HER2, including trastuzumab (Tz, a monoclonal antibody) and lapatinib (a tyrosine kinase inhibitor). HER2 inhibitors increase the survival of patients when used alone and in combination with standard chemotherapies.[6–9] Unfortunately, many patients do not initially respond to HER2 inhibitors or develop acquired resistance to these targeted agents.[9]

Tz specifically binds to the extracellular domain of HER2 and prevents activation of the intracellular HER2 tyrosine kinase. Tz has other mechanisms of action, including blockade of HER2 dimerization, increased HER2 endocytosis and degradation, and induction of antibody-dependent cellular cytotoxicity.[10,11] Tz induces cytostatic effects by arresting the cell cycle in the G1 phase and inhibits signaling involved in cell survival.[12,13] Additionally, Tz has been shown to inhibit angiogenesis and reduce the expression of growth factors, such as VEGF and transforming growth factor (TGF)-α. However, additional changes that occur in the TME, particularly changes in collagen content and organization, following Tz treatment are poorly understood.

Images of collagen within the TME can be obtained from second harmonic generation (SHG) microscopy. SHG is a nonlinear optical phenomenon in which two photons of the same wavelength are combined through a material to yield one photon with twice the energy (one-half the wavelength) of the incident photon. Collagen SHG imaging probes the fibrillar collagen content of tissues and generates photon intensity images of collagen

*Address all correspondence to: Melissa C. Skala, E-mail: m.skala@vanderbilt.edu

1083-3668/2015/$25.00 © 2015 SPIE

fibers within the tissue, which can be analyzed to assess collagen density and alignment.[14–18] Collagen fibers, such as type I, II, III, V, and XI, exhibit a strong SHG signal. In particular, increased amounts of collagen types I, III, and V have been found within breast cancers.[19,20] SHG imaging of breast cancer samples has revealed distinct collagen alignment configurations that correlate with increased tumor aggressiveness and invasion.[1–3,21] SHG images can be assessed for collagen density and relative alignment of collagen fibers. Additionally, tumor collagen can be assessed by trichrome staining of histological slides. Trichrome stains all types of collagen nondiscriminately and provides information complementary to that quantified from SHG images of fibrillar collagen. In contrast to trichrome stains, SHG microscopy can be performed *in vivo*.

Few studies have characterized changes in the TME following chemotherapy or targeted therapy. Therefore, this study investigates changes in the collagen content of HER2+ tumors following treatment with Tz. Two isogenic HER2+ breast cancer cell lines, one Tz-responsive (BT474) and the other selected for Tz resistance (HR6), were established as xenografts in athymic mice. Tumor-bearing mice treated with Tz or with a control immunoglobulin (IgG) were used to assess collagen content from SHG images *in vivo* at three time points (2, 5, and 14 days of treatment) and in histological trichrome-stained tumor sections harvested at days 2, 5, and 14. These studies tested the hypothesis that Tz treatment affects collagen in the TME, independent of the effect of Tz on the tumor cells themselves.

2 Materials and Methods

2.1 *Xenograft Model*

This study was approved by the Vanderbilt University Animal Care and Use Committee and meets the NIH guidelines for animal welfare. A total of 36 mice were used. BT474 (10^8; ATCC) and HR6 cells (10^8; Ref. 22) in 100 μL Matrigel (Corning) were injected in the inguinal mammary fat pads of six-week-old female athymic nude mice (J:NU; Jackson Laboratories). Each mouse was injected in two locations, on the right and left of the lower portion of the mammary fat pad and two tumors grew in all mice except three, which only had one tumor (tumor take rate of 96%). BT474 and HR6 cells are ER+/HER2+ isogenic cell lines. The HR6 cell line was derived from a BT474 tumor that developed resistance to Tz treatment.[22] These two cell lines were chosen because both overexpress HER2, the target protein of Tz, but only the BT474 tumors shrink in response to Tz treatment. Tumors were allowed to grow to ~150 mm^3; then the mice were randomized into control or Tz treatment groups, with nine mice in each group. Tumor-bearing mice were treated intraperitoneally with control human immunoglobulin, 10 mg/kg (IgG; R&D Systems) or Tz, 10 mg/kg (Genentech), twice weekly for two weeks (on days 0, 3, 7, and 10). This dose of Tz was chosen to mimic the therapeutic dose in patients.[23] To minimize tumor variance, age-matched mice were used, a single batch of cells for each tumor type was generated and injected, the same number of cells per tumor was injected, and treatment was initiated when the tumors were approximately the same size (~150 mm^3).

For intravital imaging, the mice were anesthetized with isofluorane and the skin overlaying the tumor was removed. The tumor was covered with a coverslip and the mouse was positioned on the microscope stage. Three locations of each tumor were imaged. Each tumor type (BT474, HR6) and group (control, Tz) at each time point (2, 5, and 14 days of treatment) consisted of three mice (six tumors). One mouse from the control and Tz-treated BT474 groups on day 2 and the Tz-treated HR6 day 2 group grew only one tumor, and therefore, those groups consisted of five tumors. Mice were humanely euthanized after imaging while under anesthesia. Tumors were collected postmortem for tissue fixation. The time points (2, 5, and 14 days) were chosen based on previous studies of these mouse tumors, which found metabolic and vascular changes within 2 and 5 days, respectively, of Tz treatment, and significant changes in tumor volume within 14 days of Tz treatment.[24,25]

2.2 *Collagen SHG Imaging*

Collagen SHG imaging was performed on a custom-built, commercial multiphoton microscope (Bruker). A 40× oil-immersion objective (1.3 NA) coupled the illumination and emission light through an inverted microscope (TiE, Nikon). A titanium: sapphire laser (Coherent Inc.) tuned to 890 nm, with an average power of 8.4 to 8.6 mW, provided the illumination light. The incident light was attenuated by a Pockel cell to vary the power of the illumination light, which results in an elliptically polarized beam. A photomultiplier tube (Hamamatsu) detected the emitted photons through a 450/35 nm notch filter. A pixel dwell time of 4.8 μs was used to collect 256 × 256 pixel images. Single-frame images for three different locations for each tumor were acquired. Each image frame was averaged eight times to reduce noise. Sequential images were separated laterally by at least one field of view, 270 μm. Images were acquired of tumor tissue ~20 to 60 μm in depth into the tumor.

2.3 *Collagen SHG Image Analysis*

Collagen alignment was quantified from the SHG images using the curvelet-based alignment analysis software, CurveAlign.[26] CurveAlign uses a fast discrete curvelet transform to find the location and edges of collagen fibers and returns orientation data and descriptive statistics. For our images, collagen alignment was assessed relative to the horizontal plane of the image. An alignment coefficient of 1 indicates parallel fibers, while 0 indicates perpendicular fibers. Collagen density was quantified by image thresholding. The histogram of pixel intensities for most images was bimodal, with one mode representing the background pixels and one mode representing the collagen fibers. Each pixel was assigned a value of 0 or 1, depending on whether the intensity value of that pixel was above (value = 1) or below (value = 0) the optimal threshold value computed for the image using Otsu's method (MATLAB®). Collagen density was quantified as the sum of the thresholded image, which represents the portion of collagen positive pixels. The collagen alignment and density outputs from the three fields of view interrogated for each tumor were averaged for a single collagen profile of each tumor.

2.4 *Trichrome Staining and Analysis*

Tumors were collected and placed in buffered formalin, paraffin embedded, sliced, and stained with trichrome. Trichrome stains multiple cellular structures, including collagen, cell cytoplasms, and cell nuclei. All types of collagen are stained with trichrome, and the resulting sections can be qualitatively analyzed. Collagen

staining was quantified from three tumors per group by expert (Rebecca S. Cook) analysis of intra- and extratumoral collagen content. Tumor collagen content was scored based on the presence and intensity of staining, with an increased score indicative of increased collagen staining. The trichrome score represents the sum of four measures, selected between 0 and 2 for each field of view analyzed: intra dense strands, intra diffuse strands, extra dense strands, and extra diffuse strands.

2.5 *Statistics*

The independence of observations between tumors was confirmed using logistic regression. Differences in collagen alignment, density, and trichrome staining were assessed between control and Tz-treated tumors within each time point and within control or Tz-treated tumors over time using nonparametric rank sum tests. We used an alpha significance level of 0.05. Correlation analysis was performed using Spearman's rank correlation coefficient.

3 Results

The collagen content of Tz-responsive (BT474) and Tz-resistant (HR6) tumors was examined by *in vivo* collagen SHG imaging and trichrome staining over a 14-day time course of control-IgG or Tz treatment. BT474 tumors respond to Tz with increased cell death and decreased tumor volume, while Tz does not induce cell death or decrease growth in HR6 tumors.[22,24,25] Collagen SHG images were analyzed using CurveAlign to extract the relative fiber alignment and density of collagen positive pixels (Fig. 1). Figure 1(c) shows the thresholded intensity mask image of collagen density, where all collagen positive pixels have a value of 1 and all negative pixels have a value of 0. Trichrome stained tumor sections were scored from 0 to 8 based on the presence and intensity of the intra- and extratumor collagen. Representative images of trichrome stained tumor sections demonstrate trichrome scoring heterogeneity [Figs. 1(d)–1(f)].

Collagen analysis revealed significant differences as a result of tumor growth and treatment with Tz in BT474 xenografts. Representative collagen SHG images demonstrate the typical size, density, and alignment of collagen fibers within control and Tz-treated BT474 tumors over the time course [Fig. 2(a)]. Collagen density was obtained from collagen SHG images as the portion of collagen positive pixels. Control BT474 tumors initially had a collagen density of 0.38 on day 2, which significantly ($p < 0.05$) increased to 0.47 on day 5 and was maintained at 0.49 on day 14 [Fig. 2(b)]. No significant differences in collagen density were detected between control and Tz-treated BT474 tumors. Likewise, no differences in collagen alignment were detected in BT474 tumors treated with Tz for two or five days. On day 14, however, there was a significant reduction in the collagen alignment of Tz-treated BT474 tumors compared with control BT474 tumors [$p < 0.05$; Fig. 2(c)]. The intratumor variance for the density of the BT474 tumors was 0.002, while the intergroup variance was 0.004, suggesting greater differences between tumors within a time point and treatment group than within individual tumors. The intratumor variance for the coefficient of alignment of collagen fibers within BT474 tumors was 0.008, while the intergroup variance was 0.02 ($p < 0.05$), again indicating greater heterogeneity between individual tumors rather than within a tumor.

Trichrome staining of collagen revealed significant differences in collagen between control and Tz-treated BT474 tumors. A trichrome staining score was assigned to each histology section based on visual analysis of the intra- and extratumoral collagen, both dense and diffuse. An increased score indicates increased collagen content. Significant reductions in collagen trichrome scores were detected on 2, 5, and 14 days ($p < 0.05$) of treatment in the BT474 tumors [Fig. 2(d)].

Representative collagen SHG images from control and Tz-treated HR6 tumors are shown in Fig. 3(a). Control HR6 tumors showed an increase in collagen density over time, from 0.38 on day 2 to 0.55 on day 14 [$p < 0.05$; Fig. 3(b)], similar to the increase in collagen density observed in the control BT474

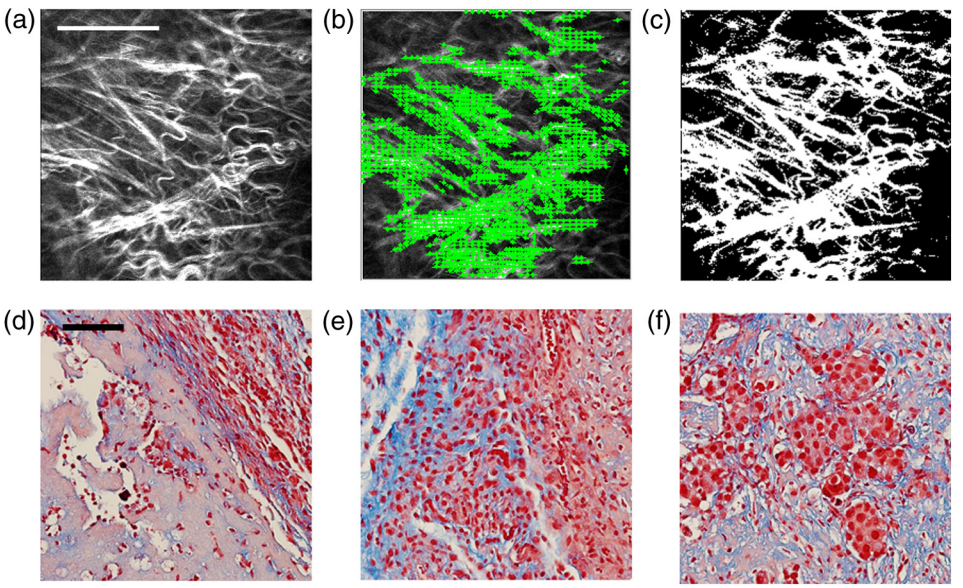

Fig. 1 (a) Original collagen second harmonic generation (SHG) image. (b) Overlay image of identified collagen fiber angles (green arrows). (c) Collagen density obtained from a thresholded image. (d) to (f) Representative trichrome images obtained at 400× to demonstrate a low [(d), score of 2], medium [(e), score of 5], and high [(f), score of 8] score. Scale bars are 100 μm.

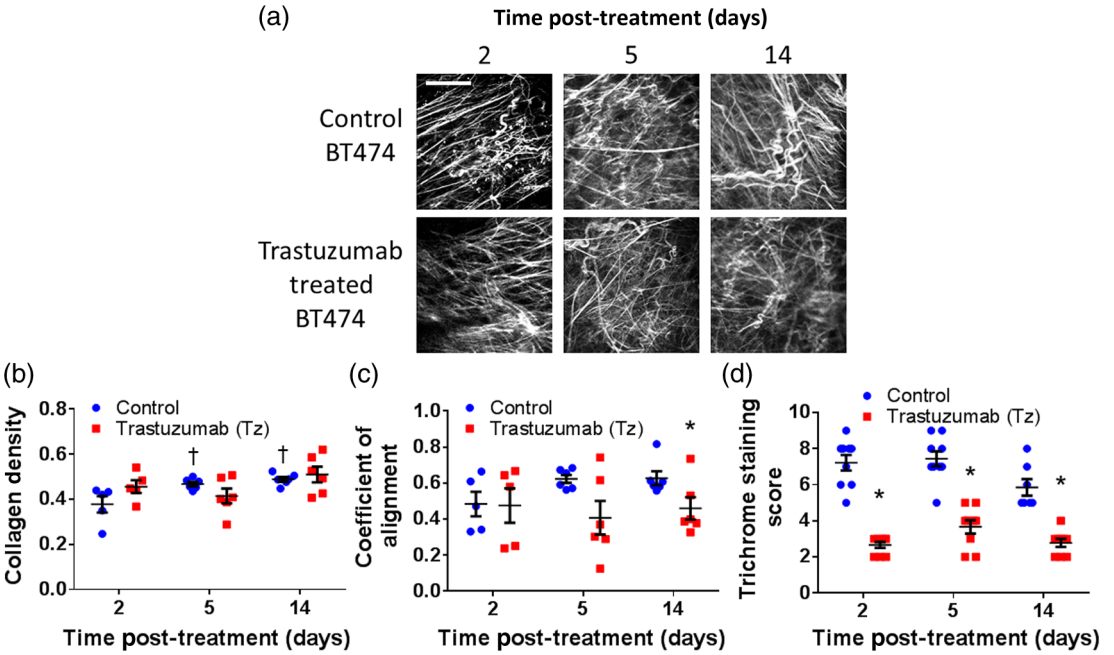

Fig. 2 (a) Representative collagen SHG images from BT474 tumors. Scale bar is 100 μm. (b) Collagen density of SHG images for control and trastuzumab (Tz)-treated BT474 tumors. (c) Coefficient of alignment of SHG images for control and Tz-treated BT474 tumors. (d) Trichrome staining score for control and Tz-treated BT474 tumors. † $p < 0.05$ versus day 2. * $p < 0.05$ versus control.

tumors over time [Fig. 2(b)]. Tz resulted in stable collagen SHG density in both the BT474 and HR6 tumors across all time points [Figs. 2(b) and 3(b)]. No significant differences in collagen density between the Tz-responsive and Tz-resistant tumors (within control and Tz-treated groups) were observed at any time point ($p > 0.05$). The intratumor variance for the collagen density of the HR6 tumors was less than the variance between HR6 tumor groups (0.003 and 0.007, respectively; $p < 0.05$). Likewise, the intratumor variance for the collagen coefficient of alignment of the HR6 tumors was less than the variance between HR6 tumor groups (0.01 and 0.02, respectively; $p < 0.05$). Tz failed to induce a decreased collagen alignment in HR6 tumors over time or between control and Tz-treated tumors [Fig. 3(c)]. A significant reduction in collagen alignment ($p < 0.05$) was detected in control HR6 tumors compared with control BT474 tumors on days 5 and 14. A significant reduction in the trichrome score was detected in Tz-treated HR6 tumors compared to control tumors at every time point [Fig. 3(d)].

Correlation analysis was performed between collagen endpoints from control BT474 and HR6 tumors using matched tumor data to investigate relationships between SHG imaging endpoints and trichrome scores. Neither the collagen density nor the coefficient of alignment determined from SHG images [Fig. 4(a)] correlated with the trichrome score. Additionally, none of the endpoints, trichrome score, SHG density, or SHG coefficient of alignment, correlated with tumor volume [Figs. 4(b)–4(d)]. The SHG density did not correlate with the coefficient of alignment [Fig. 4(e)]. However, a significant correlation was detected between SHG density and the age of the tumor [Fig. 4(f)].

4 Discussion

Tz is an HER2-targeted antibody prescribed clinically for treatment of breast cancers that overexpress HER2. While many studies have characterized the effects of Tz on the tumor epithelium, few studies have investigated the effects of Tz on the tumor microenvironment. This study investigated the effects of Tz on breast tumor collagen in both Tz-responsive and Tz-resistant tumors.

Representative collagen SHG images demonstrate the typical size, alignment, and density of collagen fibers within the tumors over time and with treatment [Figs. 1(a), 2(a), and 3(a)]. These images were acquired from a microscope system designed for multiphoton fluorescence imaging and fluorescence lifetime imaging. The only modification necessary to image collagen SHG was the addition of a narrow emission filter at one-half the wavelength of the incident near-infrared light. Collagen SHG imaging is sensitive to the polarization of the incident light. The incident light in our experimental setup is attenuated by a Pockel cell to vary the power of the illumination light, which results in an elliptically polarized beam. Therefore, we should capture collagen fibers at all angles, but the intensity of the fibers may be direction-dependent due to the polarization of the incident beam. In order to account for this bias in intensity with fiber orientation, we applied an intensity threshold to our images for further analysis so that our endpoints are independent of absolute pixel intensity. Collagen SHG images were analyzed to extract collagen density and relative fiber alignment [Figs. 2(b), 2(c), 3(b), and 3(c)].

Analysis of the collagen SHG images revealed a statistically significant increase in the density of collagen in control BT474 and HR6 tumors over time [Figs. 2(b) and 3(b)]. Correlation analysis (Fig. 4) does not show a correlation between larger tumors and collagen density. However, there is a significant correlation between SHG density and tumor age. These results suggest increased fibrillar collagen within aging tumors, which is consistent with previous reports of increased collagen content in malignant and progressing tumors.[1] Upon treatment with Tz, the BT474 tumors shrink over 14 days,[25] and the collagen density within these tumors showed no significant change over the time

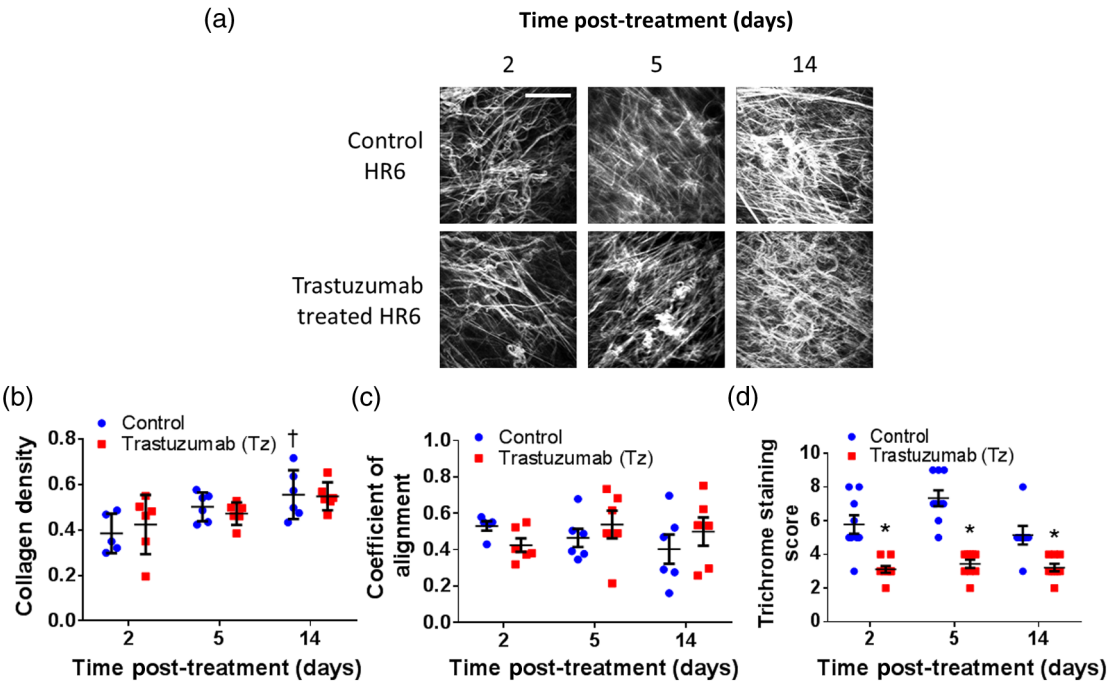

Fig. 3 (a) Representative collagen SHG images from HR6 tumors, scale bar is 100 μm. (b) Collagen density of SHG images for control and Tz-treated HR6 tumors. (c) Coefficient of alignment of SHG images for control and Tz-treated HR6 tumors. (d) Trichrome staining score for control and Tz-treated HR6 tumors. † $p < 0.05$ versus day 2. * $p < 0.05$ versus control.

course [Fig. 2(b)]. This suggests that Tz decreases the amount of fibrillar collagen in parallel with decreases in tumor volume in responsive tumors, thus maintaining constant collagen density over time.

The relative alignment of collagen fibers is associated with tumor invasion and progression, with radially aligned fibers characteristic of aggressive disease.[1–3] To assess collagen fiber alignment, a coefficient of alignment was determined for each image using CurveAlign. Images with perfectly parallel fibers would have an alignment coefficient of 1, while images with perpendicular fibers would have a value of 0. The Tz-treated BT474 tumors showed a significant decrease in coefficient of collagen alignment compared to control BT474 tumors on day 14 [Fig. 2(c)], suggesting less aggressive characteristics upon treatment with the therapeutic antibody. No change in collagen alignment was detected in the HR6 tumors treated with Tz, suggesting no significant effect of Tz on the collagen fiber alignment of these nonresponding tumors. A significant reduction in collagen alignment was detected in control HR6 tumors compared with control BT474 tumors on days 5 and 14. This may be due to differences in the characteristics and behavior of these two tumors. The HR6 tumors grow at a faster rate than the BT474 tumors, which may influence microenvironment composition.[25] HR6 cells also express higher levels of epidermal growth factor receptor and phosphorylated epidermal growth factor receptor compared to the BT474 cells,[22] which may influence tumor behavior and microenvironment composition.[27,28]

Histological analysis of collagen stained with trichrome dye revealed significant reductions in collagen content in BT474 tumors treated with Tz at all time points [Fig. 2(d)]. The trichrome staining score is a sum of four measures, diffuse and dense collagen both intra- and extratumoral, and all four individually show similar trends. Trichrome stains all forms of collagen, including fibrillar collagen. Tumors contain multiple types of collagen, including types I, II, III, and IV. Collagen type IV is particularly important within tumors because it composes the basal membrane and is involved in tumor invasion.[29,30]

The HR6 SHG and trichrome results suggest that Tz may have direct effects on the tumor microenvironment. The Tz-treated HR6 tumors did not show an increase in SHG density over the 14-day study, consistent with the Tz-treated BT474 tumors and contrary to the control HR6 and BT474 tumors [Figs. 2(b) and 3(b)]. Furthermore, the trichrome scores revealed significantly reduced scores at all time points for the Tz-treated HR6 tumors compared to the control HR6 tumors [Fig. 3(d)]. Few studies have investigated the effects of Tz treatment on non-responsive tumor cells and the tumor microenvironment. In a study of a novel glaucoma surgical intervention, Tz was tested as an antiscar agent,[31] revealing that Tz suppressed fibroblast proliferation and reduced tissue levels of TGF-β, fibroblast growth factor-β, and platelet-derived growth factor.[31] This and the HR6 results suggest that Tz may affect the collagen content of tumors by directly modifying fibroblast behavior or by modulating paracrine growth factors secreted by tumor cells. Furthermore, our previous studies of Tz effects on the tumor vasculature of BT474 and HR6 tumors revealed significant decreases in vessel oxygen saturation with five days of Tz treatment in both tumor models.[24] Our studies and these previous results suggest that Tz treatment may affect the tumor microenvironment independent of its effects on the tumor cells.

The correlation analysis (Fig. 4) indicates that the SHG endpoints, collagen density, and coefficient of alignment do not correlate with the trichrome staining score or with each other. These results agree with findings of Strupler et al. who directly compared sequential slides of collagen SHG and trichrome strain and reported that trichrome is less specific at identifying fibrillar collagen and is difficult to score and compare with SHG.[32] This

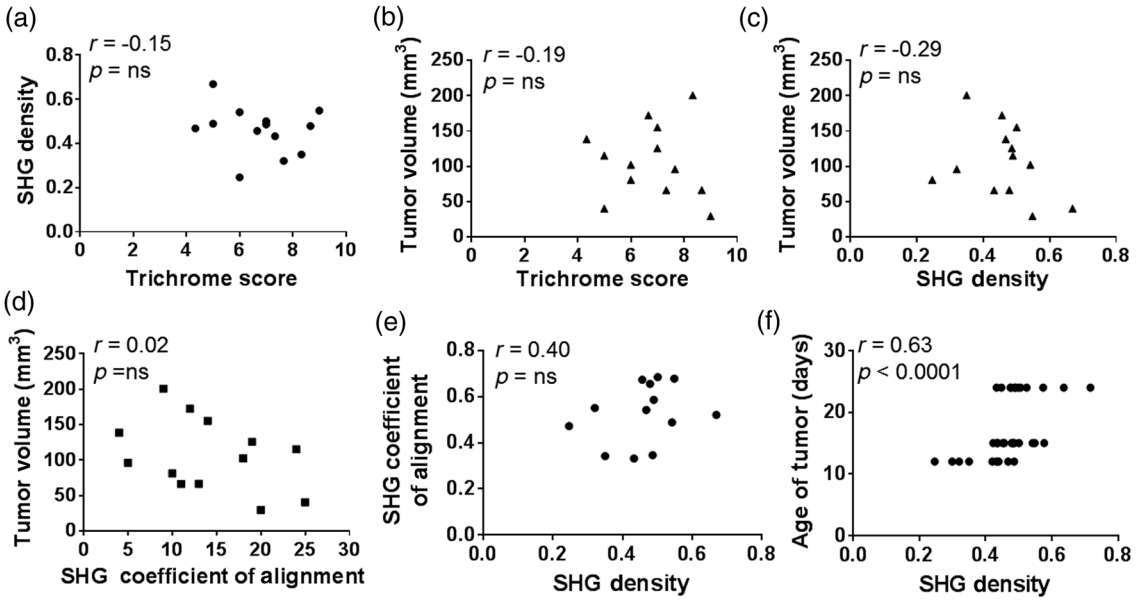

Fig. 4 (a) Correlation between trichrome score and SHG density. (b) Correlation between trichrome score and tumor volume. (c) Correlation between SHG density and tumor volume. (d) Correlation between SHG coefficient of alignment and tumor volume. (e) Correlation between SHG density and SHG coefficient of alignment. (f) Correlation between SHG density and age of tumor. *r* is Spearman's correlation coefficient. ns, not significant. Tumor volume measurements were obtained from paraffin embedded tumors, which result in tissue shrinkage.

suggests that SHG density, SHG coefficient of alignment, and trichrome score are different measurements. The inconsistencies between trichrome staining and SHG may be due to the source of contrast. Trichrome stains all collagen, including fibrillar and nonfibrillar collagen as well as other components of the ECM, while only certain fibrillar collagen strands will exhibit SHG.[32] Tumors can have increased content of nonfibrillar collagens, in particular, collagen IV,[29,30] which does not exhibit SHG.[32] Additionally, discrepancies between SHG density and trichrome staining may be due to sampling error in either the SHG measurements or trichrome imaging, both of which are limited to small fields of view and are, thus, probing only a small portion of the tumor. Imaging additional trichrome stained histological slices of the tumor or obtaining three-dimensional stacks of SHG images may provide increased representation of the tumor and more accurate measurements.

The results of this study highlight several changes in the collagen content and organization of the tumor microenvironment both in growing tumors and with Tz treatment. However, there may be confounding factors that influence the composition of the tumor microenvironment and the effectiveness of Tz. The tumor ECM can affect drug diffusion[18,33,34] and extracellular proteins, such as laminin, can co-localize with HER2 and limit the efficacy of Tz.[35] Therefore, the initial composition of the tumor ECM may influence Tz treatment. Furthermore, variability in tumor growth rates may cause variable vascular instability, which may affect the tumor microenvironment, collagen measurements, and Tz delivery and effectiveness.[36] In this study, variability across tumors was controlled by the use of a single batch of cells to initiate tumors, the use of age-matched mice, injection of the same number of cells per tumor, and the use of mouse weight to determine the Tz dose. However, some variability occurred between tumors within groups due to experimental error and biological variance. This inherent variability may mask some effects of Tz on the tumor microenvironment and may limit the effectiveness of Tz inhibition of HER2.

In conclusion, these studies suggest that Tz treatment may affect the tumor microenvironment independent of its effects on the tumor cells. We have also demonstrated that collagen SHG and histological trichrome staining analysis of collagen provide complementary endpoints of tumor collagen content and morphology. Collagen SHG imaging can be performed *in vivo* through window chambers for longitudinal studies,[24,37] while trichrome staining is inherently postmortem, potentially limiting the number of time points and increasing animal burden and expense. Trichrome staining revealed decreased collagen content in both Tz-responsive and nonresponsive tumors treated with Tz. Furthermore, collagen SHG imaging revealed similar trends in collagen density in both Tz-responsive and nonresponsive tumors treated with Tz, suggesting consistent effects of Tz on the tumor microenvironment irrespective of Tz-induced tumor size reduction. However, there was a decrease in the alignment of collagen fibers of Tz-treated responsive tumors only after 14 days of treatment. These results highlight the changes occurring within the collagen compartment of the tumor microenvironment following systemic Tz treatment.

Acknowledgments

This work was supported by funding sources that include the NCI SPORE in Breast Cancer (P50 CA098131), ASLMS Student Research Grant (A.J.W.), NSF Graduate Research Fellowship (DGE-0909667; A.J.W.), DOD Breast Cancer Research Program (DOD-BC121998), NIH (NCI R01 CA185747), and Mary Kay Foundation (067-14).

References

1. P. P. Provenzano et al., "Collagen density promotes mammary tumor initiation and progression," *BMC Med.* **6**, 11 (2008).

2. P. P. Provenzano et al., "Collagen reorganization at the tumor-stromal interface facilitates local invasion," *BMC Med.* **4**(1), 38 (2006).
3. P. P. Provenzano, K. W. Eliceiri, and P. J. Keely, "Multiphoton microscopy and fluorescence lifetime imaging microscopy (FLIM) to monitor metastasis and the tumor microenvironment," *Clin. Exp. Metastasis* **26**(4), 357–370 (2009).
4. R. K. Jain and T. Stylianopoulos, "Delivering nanomedicine to solid tumors," *Nat. Rev. Clin. Oncol.* **7**(11), 653–664 (2010).
5. J. S. Ross and J. A. Fletcher, "The HER-2/neu oncogene in breast cancer: prognostic factor, predictive factor, and target for therapy," *Stem Cells* **16**(6), 413–428 (1998).
6. H. A. Burris, III et al., "Phase I safety, pharmacokinetics, and clinical activity study of lapatinib (GW572016), a reversible dual inhibitor of epidermal growth factor receptor tyrosine kinases, in heavily pretreated patients with metastatic carcinomas," *J. Clin. Oncol.* **23**(23), 5305–5313 (2005).
7. A. M. Storniolo et al., "Phase I dose escalation and pharmacokinetic study of lapatinib in combination with trastuzumab in patients with advanced ErbB2-positive breast cancer," *J. Clin. Oncol.* **26**(20), 3317–3323 (2008).
8. M. J. Piccart-Gebhart et al., "Trastuzumab after adjuvant chemotherapy in HER2-positive breast cancer," *N. Engl. J. Med.* **353**(16), 1659–1672 (2005).
9. C. L. Vogel et al., "Efficacy and safety of trastuzumab as a single agent in first-line treatment of HER2-overexpressing metastatic breast cancer," *J. Clin. Oncol.* **20**(3), 719–726 (2002).
10. G. Valabrega, F. Montemurro, and M. Aglietta, "Trastuzumab: mechanism of action, resistance and future perspectives in HER2-overexpressing breast cancer," *Ann. Oncol.* **18**(6), 977–984 (2007).
11. C. A. Hudis, "Trastuzumab—mechanism of action and use in clinical practice," *N. Engl. J. Med.* **357**(1), 39–51 (2007).
12. S. Mayfield, J. P. Vaughn, and T. E. Kute, "DNA strand breaks and cell cycle perturbation in herceptin treated breast cancer cell lines," *Breast Cancer Res. Treat.* **70**(2), 123–129 (2001).
13. M. Cuello et al., "Down-regulation of the ErbB-2 receptor by trastuzumab (herceptin) enhances tumor necrosis factor-related apoptosis-inducing ligand-mediated apoptosis in breast and ovarian cancer cell lines that overexpress ErbB-2," *Cancer Res.* **61**(12), 4892–4900 (2001).
14. X. Y. Chen et al., "Second harmonic generation microscopy for quantitative analysis of collagen fibrillar structure," *Nat. Protoc.* **7**(4), 654–669 (2012).
15. P. J. Campagnola et al., "Three-dimensional high-resolution second-harmonic generation imaging of endogenous structural proteins in biological tissues," *Biophys. J.* **82**(1), 493–508 (2002).
16. W. R. Zipfel et al., "Live tissue intrinsic emission microscopy using multiphoton-excited native fluorescence and second harmonic generation," *Proc. Natl. Acad. Sci. U S A* **100**(12), 7075–7080 (2003).
17. G. Cox et al., "3-dimensional imaging of collagen using second harmonic generation," *J. Struct. Biol.* **141**(1), 53–62 (2003).
18. E. Brown et al., "Dynamic imaging of collagen and its modulation in tumors in vivo using second-harmonic generation," *Nat. Med.* **9**(6), 796–800 (2003).
19. S. Kauppila et al., "Aberrant type I and type III collagen gene expression in human breast cancer in vivo," *J. Pathol.* **186**(3), 262–268 (1998).
20. S. H. Barsky et al., "Increased content of type-V collagen in desmoplasia of human-breast carcinoma," *Am. J. Pathol.* **108**(3), 276–283 (1982).
21. P. P. Provenzano et al., "Nonlinear optical imaging and spectral-lifetime computational analysis of endogenous and exogenous fluorophores in breast cancer," *J. Biomed. Opt.* **13**(3), 031220 (2008).
22. C. A. Ritter et al., "Human breast cancer cells selected for resistance to trastuzumab in vivo overexpress epidermal growth factor receptor and ErbB ligands and remain dependent on the ErbB receptor network," *Clin. Cancer Res.* **13**(16), 4909–4919 (2007).
23. M. S. Gee et al., "Human breast cancer tumor models: molecular imaging of drug susceptibility and dosing during HER2/neu-targeted therapy," *Radiology* **248**(3), 925–935 (2008).
24. D. R. McCormack et al., "In vivo hyperspectral imaging of microvessel response to trastuzumab treatment in breast cancer xenografts," *Biomed. Opt. Express* **5**(7), 2247–2261 (2014).
25. A. J. Walsh et al., "Optical metabolic imaging identifies glycolytic levels, subtypes, and early-treatment response in breast cancer," *Cancer Res.* **73**(20), 6164–6174 (2013).
26. Y. Liu, J. Bredfeldt, and C. Pehlke, "CurveAlign," 2013, http://loci.wisc.edu/software/curvealign (2013).
27. M. Laato et al., "Epidermal growth factor increases collagen production in granulation tissue by stimulation of fibroblast proliferation and not by activation of procollagen genes," *Biochem. J.* **247**(2), 385–388 (1987).
28. A. Buckley et al., "Sustained release of epidermal growth factor accelerates wound repair," *Proc. Natl. Acad. Sci. U S A* **82**(21), 7340–7344 (1985).
29. E. Ioachim et al., "Immunohistochemical expression of extracellular matrix components tenascin, fibronectin, collagen type IV and laminin in breast cancer: their prognostic value and role in tumour invasion and progression," *Eur. J. Cancer* **38**(18), 2362–2370 (2002).
30. J. P. Kim et al., "Human keratinocyte migration on type-IV collagen—roles of heparin-binding site and alpha-2-beta-1 integrin," *Lab Invest.* **71**(3), 401–408 (1994).
31. B. Turgut et al., "Impact of trastuzumab on wound healing in experimental glaucoma surgery," *Clin. Exp. Ophthalmol.***43**(1), 67–76 (2015).
32. M. Strupler et al., "Second harmonic imaging and scoring of collagen in fibrotic tissues," *Opt. Express* **15**(7), 4054–4065 (2007).
33. P. A. Netti et al., "Role of extracellular matrix assembly in interstitial transport in solid tumors," *Cancer Res.* **60**(9), 2497–2503 (2000).
34. C. L. Davies et al., "Comparison of IgG diffusion and extracellular matrix composition in rhabdomyosarcomas grown in mice versus in vitro as spheroids reveals the role of host stromal cells," *Br. J. Cancer* **86**(10), 1639–1644 (2002).
35. I. Beyer et al., "Controlled extracellular matrix degradation in breast cancer tumors improves therapy by trastuzumab," *Mol. Ther.* **19**(3), 479–489 (2011).
36. J. R. Less et al., "Microvascular architecture in a mammary carcinoma: branching patterns and vessel dimensions," *Cancer Res.* **51**(1), 265–273 (1991).
37. S. Q. Shan, B. Sorg, and M. W. Dewhirst, "A novel rodent mammary window of orthotopic breast cancer for intravital microscopy," *Microvasc. Res.* **65**(2), 109–117 (2003).

Alex J. Walsh is a PhD candidate at Vanderbilt University in the Department of Biomedical Engineering.

Rebecca S. Cook is an assistant professor of Cancer Biology at Vanderbilt University.

Jae H. Lee is an undergraduate student at Vanderbilt University working towards completion of his BE in biomedical engineering.

Carlos L. Arteaga is a professor of medicine and the director of the Breast Cancer Program at Vanderbilt University.

Melissa C. Skala is an assistant professor of biomedical engineering at Vanderbilt University.